




# Engineering lithium-ion battery cathodes for high-voltage applications using electromagnetic excitation

Laisuo Su<sup>1</sup>, Shikhar Krishn Jha<sup>1</sup>, Xin Li Phuah<sup>2</sup>, Jiang Xu<sup>3</sup>, Nathan Nakamura<sup>1</sup>, Haiyan Wang<sup>2</sup>, John S. Okasinski<sup>4</sup>, and B. Reeja-Jayan<sup>1,\*</sup> 

<sup>1</sup>Department of Mechanical Engineering, Carnegie Mellon University, Pittsburgh, PA, USA

<sup>2</sup>School of Materials Engineering, Purdue University, West Lafayette, IN, USA

<sup>3</sup>Civil and Environmental Engineering, Carnegie Mellon University, Pittsburgh, PA, USA

<sup>4</sup>Advanced Photo Source, Argonne National Laboratory, Lemont, IL, USA

Received: 16 January 2020

Accepted: 22 May 2020

Published online:  
28 May 2020

© Springer Science+Business  
Media, LLC, part of Springer  
Nature 2020

## ABSTRACT

Microwave radiation (MWR), a type of electromagnetic excitation source, reduces the synthesis temperature and processing time for chemical reactions compared to traditional synthesis methods. Recently, we demonstrated that MWR can engineer ceramics with different crystal phases compared to traditional methods [*Journal of Materials Chemistry A* 5, 35 (2017)]. In this study, we further apply the MWR-assisted technique to improve the electrochemical performance of LiCoO<sub>2</sub> cathodes by engineering TiO<sub>2</sub> and ZrO<sub>2</sub> ceramic coatings. Electrochemical tests suggest that the TiO<sub>2</sub> coating improves the rate capability of the LiCoO<sub>2</sub> electrode. Both TiO<sub>2</sub> and ZrO<sub>2</sub> coatings improve the high-voltage (4.5 V) cycling stability of LiCoO<sub>2</sub>. The capacity remaining is improved from 52.8 to 84.4% and 81.9% by the TiO<sub>2</sub> coating and the ZrO<sub>2</sub> coating, respectively, after 40 cycles. We compare these results with existing studies that apply traditional methods to engineer TiO<sub>2</sub>/ZrO<sub>2</sub> on LiCoO<sub>2</sub>, and find that the MWR-assisted method shows better performance improvement. X-ray photoelectron spectroscopy measurements suggest that the improved cycling stability arises from the formation of metal fluorides that protect the electrode from side reactions with electrolytes. This mechanism is further supported by the reduced Co dissolution from TiO<sub>2</sub>/ZrO<sub>2</sub>-coated LiCoO<sub>2</sub> electrode after cycling. This study provides a new toolbox facilitating the integration of many delicate, low melting point materials like polymers into battery electrodes.

Address correspondence to E-mail: [bjayan@andrew.cmu.edu](mailto:bjayan@andrew.cmu.edu)

## Introduction

Engineering the surface of battery electrodes is crucial to improve their electrochemical performance as many important reactions happened at this region, including electrolytes decomposition, transition metal dissolution, and  $\text{Li}^+$  and  $\text{e}^-$  combination [1, 2]. Many inorganic components have been widely explored as the coating agents, like  $\text{Al}_2\text{O}_3$  [1, 3],  $\text{ZnO}$  [4],  $\text{Al}_2\text{O}_3$ -doped  $\text{ZnO}$  [5],  $\text{TiO}_2$  [6], and  $\text{Li}_3\text{PO}_4$  [7]. These coatings improve the cycling stability of battery electrodes by alleviating electrolyte decomposition and reducing the generation of irreversible solid electrolyte interphase (SEI). However, simple metal oxides/phosphates coatings could increase impedance over cycling and decrease rate capability because of their insulating nature toward  $\text{Li}$ -ions [1]. In addition, most of existing coating techniques require high temperature and/or low vacuum conditions that increase the complexity and cost for the battery manufacturing process [8]. Therefore, exploring novel techniques to engineer battery electrodes warrants further investigate.

Electromagnetic (EM) radiation can aid in synthesizing and crystallizing of both inorganic and organic materials due to their ability to reduce the processing temperature and shorten the processing time [9, 10]. One of the most widely studied forms of EM radiation for materials synthesis is microwave radiation (MWR), with frequency in the range of 0.3–300 GHz. Compared to conventional furnace-based synthesis methods, the MWR-assisted technique can synthesize inorganic/organic compounds at much shorter times and with higher yields [11–14]. Moreover, the MWR-assisted method generates ceramics with unique crystal structures. For example, Nakamura et al. found that  $\text{TiO}_2$  films grown under MWR exposure contain a different phase composition and increased crystallinity compared to those grown at similar temperatures using a furnace-heating method without EM fields [11].

Despite the widespread exploration of the MWR-assisted method in materials synthesis, applying such filed-assisted techniques in lithium-ion batteries (LIBs) has not attracted much attention. For example, Kim et al. applied the MWR-assisted method to engineer  $\text{FePO}_4$  on the surface of  $\text{LiCoO}_2$  cathode electrode and improved its 4.7 V high-voltage cycling stability [15]. However, no follow-up studies were

done to explore the effect of other MWR synthesized ceramics or polymers on the electrochemical performance of  $\text{LiCoO}_2$  or other cathodes. Nevertheless, many inorganic and organic materials have been synthesized using the MWR-assisted technique [16]. Additionally, many experimental parameters, like microwave power and heating rate, affect the final products during the MWR-assisted synthesis, and will therefore affect the electrochemical performance of battery electrodes. Systematically investigating all these parameters and identifying their optimal combination is not trivial. Accord, further investigations are needed to explore the MWR-assisted technique as a surface engineering technique for battery electrodes.

In this study, we applied MWR to engineer  $\text{TiO}_2$  and  $\text{ZrO}_2$  on the surface of  $\text{LiCoO}_2$  electrodes.  $\text{TiO}_2$  and  $\text{ZrO}_2$  were selected for the first step of study because of their widely applications [17, 18]. They have also been proved to improve electrochemical performance of many battery electrodes [19]. We chose  $\text{LiCoO}_2$  because of its high theoretical capacity and good rate performance. In situ synchrotron X-ray diffraction (XRD) technique was applied to monitor the growth of  $\text{ZrO}_2$  and  $\text{TiO}_2$  on the surface of  $\text{LiCoO}_2$  particles. The effect of the coatings on the rate capability and 4.5 V high-voltage cycling stability was then investigated. Our study demonstrates that the MWR-assisted technique can become a versatile tool to engineer the surface of battery cathode electrodes. Exploring other coating materials, including both inorganic ceramics and organic polymers, and applying them to advanced cathode materials warrants further investigations for designing next-generation LIBs with high energy and power density as well as extended lifespan.

## Materials and methods

### In situ synchrotron X-ray diffraction characterization

MWR-assisted synthesis experiments were performed using an Anton Paar Monowave 300 reactor operating at 2.45 GHz. The picture of the microwave reactor is shown in Fig. S1 in supporting information (SI).  $\text{LiCoO}_2$  powder was purchased from MTI cooperation. All other chemicals were purchased from VWR cooperation and used without further

purification. Three in situ experiments were conducted: (1) MWR heating of LiCoO<sub>2</sub> powder, (2) MWR-assisted synthesis of TiO<sub>2</sub> coatings on LiCoO<sub>2</sub> powder, and (3) MWR-assisted synthesis of ZrO<sub>2</sub> coatings on LiCoO<sub>2</sub> powder. For the MWR-heating experiment, 200 mg of LiCoO<sub>2</sub> powder was dispersed in a 5 mL tetraethyl glycol (TEG) solution and heated up to 250 °C at the rate of 1.5 °C/min (the slowest rate that can be achieved by the microwave reactor), held at that temperature for 10 min, and cooled to 55 °C. The solution was stirred at 650 rpm to avoid hotspot formation. For the other experiments, where TiO<sub>2</sub> and ZrO<sub>2</sub> coatings were synthesized on LiCoO<sub>2</sub> powder, sol-gel solutions based on titanium(IV) butoxide and zirconium(IV) tert-butoxide were used as TiO<sub>2</sub> and ZrO<sub>2</sub> precursors, respectively [20]. The sol-gel was mixed with TEG in the ratio of 1:4 by volume. 200 mg of LiCoO<sub>2</sub> powder was dispersed in a total of 5 ml precursor solution, which was then heated in the microwave reactor using identical experimental conditions as the MWR-heating experiment.

Figure S1 shows a schematic of the in situ synchrotron XRD experiments that were conducted at the 6-ID-D beamline at the Advanced Photon Sources, Argonne National Laboratory. A monochromatic X-ray beam of energy 80 keV was used for diffraction, which allows for X-ray transmission through the thick walls of glass vials. A 2-D PerkinElmer amorphous silicon area detector with cesium iodide scintillator was used to collect 2D diffraction patterns. Because of the high absorption of X-rays by glass vials, an acquisition rate of 1 min was used for data collection. This rate achieved an acceptable signal-to-noise ratio; the ceramic oxide diffraction peaks could be distinguished from the background signal caused by the glass vial and solution while considering the temporal resolution of the chemical reaction. The microwave reactor was modified to include inlet and outlet ports allowing X-rays to pass through and reach the glass vial. Fit2D was utilized to convert 2D detector images to intensity-2 theta angle relationships. High-order polynomial functions were applied to remove the solution and glass vial background via MATLAB [21, 22]. The remaining peaks were then identified and individually fit to Gaussian peaks to obtain peak locations, intensities, and full-width at half maxima (FWHM).

### MWR-assisted method to synthesize TiO<sub>2</sub> and ZrO<sub>2</sub> coating on LiCoO<sub>2</sub> surface for LIB electrodes

To engineer TiO<sub>2</sub> and ZrO<sub>2</sub> on the surface of LiCoO<sub>2</sub> powder, 500 mg of LiCoO<sub>2</sub> powder was dispersed in a 12 ml solution comprising of 9 ml TEG and 3 ml sol-gel solution. TiO<sub>2</sub> synthesis was performed using experimental conditions of 150 °C–200 W–10 min–1 min, where 150 °C represented the maximum temperature, 200 W was the maximum microwave power applied, 10 min was the heating time to reach the maximum temperature, and 1 min was the hold time at the maximum temperature [11]. The vial was cooled down to 55 °C by forced air cooling after the experiment. The experimental conditions for MWR-assisted ZrO<sub>2</sub> synthesis were 225 °C–200 W–30 min–min [23]. The obtained powder was washed three times with deionized water and then dried at 80 °C in a vacuum chamber overnight. The dried powder was subsequently annealed at 750 °C for 6 h in air, followed by air cooling to room temperature.

### Material characterization

Transmission electron microscopy (TEM) imaging was used to characterize the TiO<sub>2</sub> and ZrO<sub>2</sub> coatings on LiCoO<sub>2</sub> powder. The synthesized powder was dispersed in ethanol, dropped onto TEM grids, and dried overnight before being loaded for imaging. TEM characterization was performed using a FEI Talos F200X operated at 200 kV. Energy-dispersive X-ray spectroscopy (EDS) data were collected by ChemiSTEM technology (X-FED and SuperX EDS) using four silicon drift detectors.

X-ray photoelectron spectroscopy (XPS) measurements were done on a Thermo Fisher ESCALAB 250Xi with an X-ray source of monochromatized Al K  $\alpha$  radiation (1486.7 eV). The base pressure was 10<sup>-8</sup> Pa, and the spot diameter was 600  $\mu$ m. Five survey scans with a step size of 1.0 eV were collected, followed by ten high-resolution scans with a step size of 0.1 eV for target elements. The obtained XPS spectra were analyzed by AVENTAGE software with the following parameters: FWHM (eV) = 0.5:3.5 and Lorentzian/Gaussian of 0.3. In the XPS depth profiling analysis, Ar<sup>+</sup> ion beam was applied on an area of 3 mm\*3 mm for the etching process, followed by XPS data collection for specific elements. The Ar<sup>+</sup> gun was operated at 3 keV and the etching time was 15 s

for each step. A total of 50 steps were applied on each sample for the depth profiling analysis.

The weight percentages of Co, Ti, and Zr in  $\text{LiCoO}_2$  powder were measured by inductively coupled plasma mass spectrometry (ICP-MS, Agilent Technologies 7700 Series). Briefly, 7.3 mg of  $\text{TiO}_2$ -coated  $\text{LiCoO}_2$  powder or 9.6 mg of  $\text{ZrO}_2$ -coated  $\text{LiCoO}_2$  powder was added into 15-ml centrifuge tube containing 5 ml HCl (37%). The tubes were sealed and rotated on an end-over-end rotator (30 rpm) overnight. Then, the solution was diluted by 2000 times. 6 ml of the solution was filtered through a 0.45- $\mu\text{m}$  filter, and 0.2 ml of trace metal grade  $\text{HNO}_3$  (69%) was added to acidize the solution. Mixed standards of 0, 10, 20, 50, 100, 250, and 500 ppb for different elements with the same percentage of  $\text{HNO}_3$  ( $\sim 5\%$ ) as the samples were used for calibration.

To study the Co dissolution from  $\text{LiCoO}_2$  electrodes after cycling, coin cells were disassembled in an argon-filled glove box with  $\text{O}_2$  and  $\text{H}_2\text{O}$  level below 0.5 ppm. All components were immersed in 10 ml dimethyl carbonate (DMC) for 3 days. 2 ml of the solution was then diluted in 6 ml  $\text{HNO}_3$  (65%). The mixed solution was heated to 120 °C in a vacuum chamber until all liquid disappeared. The remaining white/yellow powder was collected and dissolved in 10 ml deionized water, followed by 30 min of ultrasonic treatment. Finally, 6 ml solution was filtered through a 0.45- $\mu\text{m}$  filter, and 0.2 ml  $\text{HNO}_3$  (70%) was added to the solution before conducting the ICP-MS measurement.

### Electrode preparation, coin cell fabrication, and testing

$\text{LiCoO}_2$  powder with and without the  $\text{TiO}_2/\text{ZrO}_2$  coating was mixed with carbon black and polyvinylidene fluoride in N-methyl pyrrolidone with a ratio of 8:1:1 by weight. The slurry was then spread on an aluminum foil current collector and dried in a vacuum chamber at 110 °C overnight to remove the solvent and moisture. 14-mm-diameter cathode disks were punched and collected in glass bottles, with a typical mass loading of 4–5 mg. CR-2016 type coin cells were fabricated using these disks as the cathode and lithium chips as the anode. Celgard separators and lithium chips were purchased from MTI Corporation, while electrolytes were purchased from Sigma-Aldrich. The electrolyte was ethylene carbonate/ethyl methyl ethyl carbonate (50/

50, v/v) containing 1 M  $\text{LiPF}_6$ . The entire assembly process was carried out in an argon-filled glovebox with  $\text{O}_2$  and  $\text{H}_2\text{O}$  level maintained below 0.5 ppm.

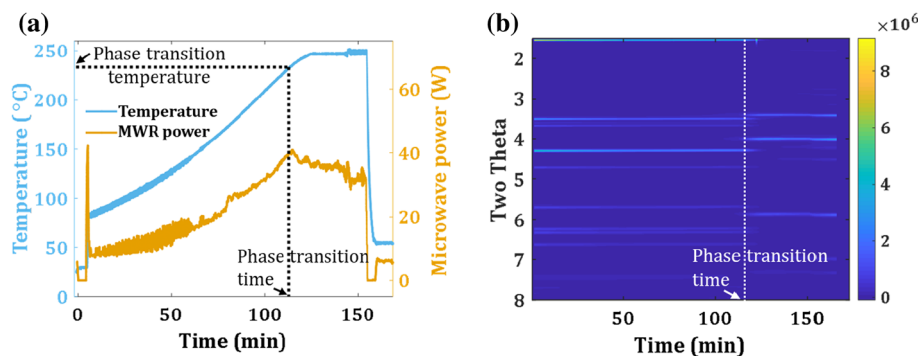
Electrochemical performance of  $\text{LiCoO}_2$  electrodes was measured using Biologic VMP3 (BioLogic Science Instruments) and LAND battery cyclers (LAND Electronics Co., Ltd.). After assembling, all cells went through a formation process consisting of three continuous cycles at C/10 (1C = 145 mA/g) within 3.0–4.2 V at room temperature. Rate capability was studied by charging cells at C/3 using constant current (CC)–constant voltage (CV) protocol, followed by different discharging rates, including C/10, C/3, 1C, 2C, 5C, and 10C. The cutoff current during the CV charging process was C/100 to ensure that all cells were discharged at the same status. Galvanostatic intermittent titration technique (GITT) measurement was conducted by applying a 30-min galvanostatic charge/discharge pulse (C/10), followed by a 2-h relaxation. Electrochemical impedance spectroscopy (EIS) was tested at room temperature. Before the EIS measurement, cells were charged to 4.0 V using a CC-CV protocol with C/100 as the cutoff current during the CV process. The impedance was then potentiostatically measured by applying an AC voltage of 10 mV amplitude over the frequency range of 100 kHz to 10 mHz. High-voltage cycling test was conducted at room temperature by cycling cells at C/2 within the voltage range of 3.0–4.5 V using a CC protocol for both charging and discharging processes.

## Results

### Material characterization

Many microwave processing parameters affect the final synthesized products, including maximum temperature, maximum microwave power, heating rate, and hold time at the maximum temperature. The maximum temperature was determined based on the results from the in situ synchrotron XRD experiment, as shown in Fig. 1. Figure 1a shows the temperature and power profiles of the microwave system during the MWR-assisted heating of  $\text{LiCoO}_2$ . The corresponding two-dimensional contour plot for the structure of  $\text{LiCoO}_2$  powder is displayed in Fig. 1b. At around 115 min, we found significant shifts of two-theta values in the XRD pattern, suggesting a

**Figure 1** In situ synchrotron X-ray diffraction (XRD) results. **a** Temperature and power profile during in situ synchrotron XRD experiment for LiCoO<sub>2</sub> powder in TEG solution. **b** The evolution of 2θ values for the diffraction pattern during in situ XRD experiment.



new phase formed because of the microwave heating. Figure S2 suggests the new phase is cubic CoO [24]. The formation of cubic CoO started at 230 °C. Therefore, the maximum temperature for engineering TiO<sub>2</sub> and ZrO<sub>2</sub> coatings on the surface of LiCoO<sub>2</sub> was set below 230 °C to avoid any such phase transformation of LiCoO<sub>2</sub> during the MWR processing. Although other parameters, like the heating rate and the hold time, affected the synthesized TiO<sub>2</sub> and ZrO<sub>2</sub>, these parameters were not systematically studied and were chosen based on empirical trials [20]. Optimizing these parameters is not trivial and warrants further investigations.

TiO<sub>2</sub> and ZrO<sub>2</sub> coatings on LiCoO<sub>2</sub> were studied using TEM, scanning transmission electron microscopy (STEM), EDS, and XPS. It has been reported that localized hot spots can form in LiCoO<sub>2</sub> due to MWR absorption, which may promote TiO<sub>2</sub>/ZrO<sub>2</sub> nucleation [15]. Figure 2a, b, c shows TEM image of a pristine LiCoO<sub>2</sub> particle, a TiO<sub>2</sub>-coated LiCoO<sub>2</sub> particle, and a ZrO<sub>2</sub>-coated LiCoO<sub>2</sub> particle, respectively. No obvious films could be identified in Fig. 2b, while a thin layer is shown in Fig. 2c. However, the thin layer was proven to be carbon rather than ZrO<sub>2</sub>, as shown in Fig. S3. The EDS results in Fig. 2d, e show that Ti is uniformly distributed on the surface of LiCoO<sub>2</sub> powder, while Zr nucleated at a few regions on the edge of LiCoO<sub>2</sub> particles. Three different locations were tested to statistically study the distribution of Ti and Zr on LiCoO<sub>2</sub> particles, as displayed in Fig. S4 (SI). The result shows that Ti uniformly distributed on the surface of LiCoO<sub>2</sub> particles in all cases except one particle (Fig. S4c), while Zr nucleated at a few regions on the edge of LiCoO<sub>2</sub> particles in all cases. To further examine the existence of TiO<sub>2</sub> and ZrO<sub>2</sub>, XPS was collected on both TiO<sub>2</sub>-coated and ZrO<sub>2</sub>-coated LiCoO<sub>2</sub> samples, as shown in Fig. S5. A Ti 2p<sub>3/2</sub> peak at 458.4 eV and a Zr 3d<sub>5/2</sub> peak at

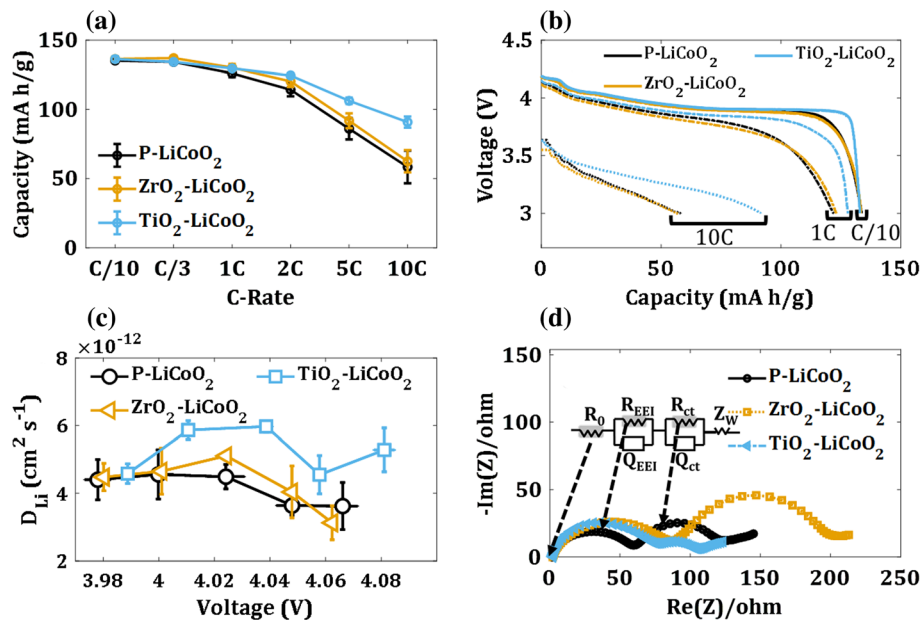
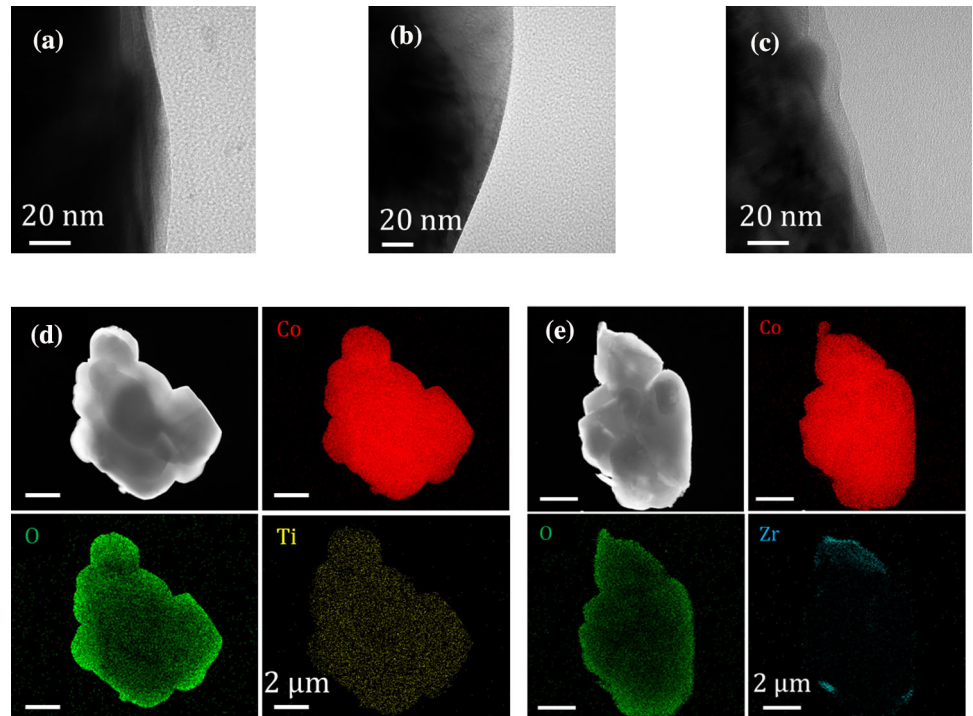
181.9 eV could be identified, proving the existence of Ti and Zr on the surface of TiO<sub>2</sub>-coated and ZrO<sub>2</sub>-coated LiCoO<sub>2</sub> powder, respectively. Based on these results, we demonstrate that TiO<sub>2</sub> and ZrO<sub>2</sub> were successfully synthesized on the surface of LiCoO<sub>2</sub> powder using the MWR-assisted technique.

Table S1 shows that the weight percentage of Co in both TiO<sub>2</sub>-coated LiCoO<sub>2</sub> and ZrO<sub>2</sub>-coated LiCoO<sub>2</sub> powder was very close to the theoretical value of Co in LiCoO<sub>2</sub> (60.2%). Additionally, the weight percentages of Ti and Zr in the powder were less than 1%. This result suggests that the weight percentages of TiO<sub>2</sub> and ZrO<sub>2</sub> in these TiO<sub>2</sub> and ZrO<sub>2</sub>-coated LiCoO<sub>2</sub> powders were negligible. Therefore, the TiO<sub>2</sub> and ZrO<sub>2</sub> coatings should have little effect on the specific capacity of LiCoO<sub>2</sub> electrodes.

### Influence of MWR-synthesized TiO<sub>2</sub>/ZrO<sub>2</sub> coatings on rate capability of LiCoO<sub>2</sub> electrodes

Figure 3 illustrates the effect of TiO<sub>2</sub> and ZrO<sub>2</sub> coatings on the rate capability of the LiCoO<sub>2</sub> electrode. The ZrO<sub>2</sub> coating had little effect on the rate capability, while the TiO<sub>2</sub> coating improved rate capability. The effect of coatings on the rate performance becomes more obvious at high rate. Figure 3a indicates that the discharge capacity of the LiCoO<sub>2</sub> electrode increased by around 50% (from 60 to 90 mA h g<sup>-1</sup>) after the TiO<sub>2</sub> coating at 10C. In comparison, the ZrO<sub>2</sub> coating did not affect the discharge capacity of the LiCoO<sub>2</sub> electrode in the rate range we measured. Figure 3b compares discharge curves of different LiCoO<sub>2</sub> electrodes at C/10, 1C, and 10C. The discharge curves of the ZrO<sub>2</sub>-coated LiCoO<sub>2</sub> and the pristine LiCoO<sub>2</sub> electrode almost overlapped each other at all the three C-rates, while the TiO<sub>2</sub>-coated LiCoO<sub>2</sub> electrode behaved differently. At low C-rates

**Figure 2** TEM images of **a** a pristine  $\text{LiCoO}_2$  particle, **b** a  $\text{TiO}_2$ - $\text{LiCoO}_2$  particle and **c** a  $\text{ZrO}_2$ - $\text{LiCoO}_2$  particle. **d** STEM image and EDS of a  $\text{TiO}_2$ - $\text{LiCoO}_2$  particle. **e** STEM image and EDS of a  $\text{ZrO}_2$ - $\text{LiCoO}_2$  particle.



**Figure 3** Rate performance of different  $\text{LiCoO}_2$  electrodes. **a** Specific capacity of  $\text{LiCoO}_2$  electrodes with respect to discharging rate. Three cells were tested for each case and the result was averaged from all cells. **b** Comparison of discharge curves of  $\text{LiCoO}_2$  electrodes at C/10, 1C, and 10C. **c** Diffusion

(C/10 and 1C), the discharge curves of the  $\text{TiO}_2$ -coated  $\text{LiCoO}_2$  electrode overlapped the pristine  $\text{LiCoO}_2$  electrode at the initial stage of the discharging. However, the voltages stayed much higher when

coefficient of Li in  $\text{LiCoO}_2$  during lithiation (charging) at around 4.0 V for different electrodes using GITT method. **d** EIS plots of different  $\text{LiCoO}_2$  electrodes. The figure inset shows a second-order ECM that is used to fit the impedance.

it closed to the end of the discharging before quickly dropped to 3.0 V. At the high C-rate (10C), the  $\text{TiO}_2$ -coated  $\text{LiCoO}_2$  electrode showed higher voltage ( $\sim 0.2$  V) during the entire discharging process and

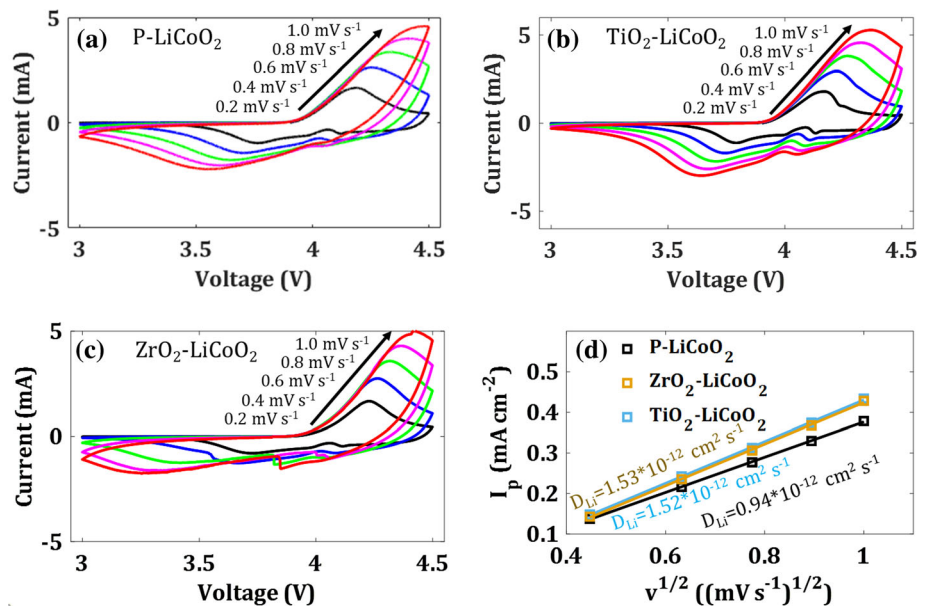
40 mA h g<sup>-1</sup> larger specific capacity than the pristine LiCoO<sub>2</sub> electrode.

The rate performance of the LiCoO<sub>2</sub> electrode could be affected by the kinetics of lithium transport in the electrode. We applied GITT to study the effect of TiO<sub>2</sub>/ZrO<sub>2</sub> coating on the transport of lithium in LiCoO<sub>2</sub>. The details of the measurement process can be found in Fig. S6, which suggests that the diffusion coefficient of lithium in LiCoO<sub>2</sub> varied little in the voltage range of 4.0–4.4 V. Additionally, the diffusion coefficients during the charge and discharge processes were similar in value. Therefore, we only measured the diffusion coefficient of lithium in LiCoO<sub>2</sub> during the charge process at around 4.0 V for TiO<sub>2</sub>-coated and ZrO<sub>2</sub>-coated LiCoO<sub>2</sub> electrodes. Figure 3c compares the lithium diffusion coefficient in the three types of LiCoO<sub>2</sub> electrodes. The results suggest that the diffusion coefficients were in the same order of magnitude. However, the TiO<sub>2</sub>-coated LiCoO<sub>2</sub> electrode had slightly higher diffusion coefficients ( $\sim 5.5 \times 10^{-12}$  cm<sup>2</sup>s<sup>-1</sup>) compared with the pristine LiCoO<sub>2</sub> electrode ( $\sim 4.0 \times 10^{-12}$  cm<sup>2</sup>s<sup>-1</sup>). This agreed with the improved discharge performance of the TiO<sub>2</sub>-coated LiCoO<sub>2</sub> electrode seen in Fig. 3b. Figure 4 compares the diffusion coefficient of Li in different LiCoO<sub>2</sub> electrodes measured from cyclic voltammetry (CV). The voltage swapping rate was varied from 0.2 to 1.0 mV/s, during which the current was monitored. Figure 4 suggests that the peak current (*I*<sub>p</sub>) linearly increased with the square root of voltage swapping rate (*v*<sup>1/2</sup>). By applying Randles–

Sevcik equation, we calculated the diffusion coefficient of Li in different LiCoO<sub>2</sub> electrodes [6]. The result suggests that both TiO<sub>2</sub> and ZrO<sub>2</sub> coatings increased the diffusion coefficient of Li. Because the order of magnitude in the difference between these diffusion coefficients was small, more investigations are needed before drawing a clear conclusion.

EIS measurements were also conducted to study the effect of these coatings on the impedance of the LiCoO<sub>2</sub> electrode. The impedance of a coin cell is very sensitive to the fabrication process. Cells with the same type of LiCoO<sub>2</sub> electrode could have different impedance values, as shown in Fig. S7 (SI). However, the overall trend suggests that the TiO<sub>2</sub> coating reduced the impedance, while the ZrO<sub>2</sub> coatings increased the impedance, as shown in Fig. 3d. To quantitatively analyze these results, the impedances were fitted using a second-order equivalent circuit model (ECM), as shown in the inset in Fig. 3d. The *R*<sub>0</sub> represents the ohmic resistance, the *R*<sub>EEL</sub> and *Q*<sub>EEL</sub> represent the resistance and the phase constant element of the EEL layer, and the *R*<sub>ct</sub> and *Q*<sub>ct</sub> represent the resistance and the phase constant element charge-transfer process. The fitted results in Table S2 suggest that the ZrO<sub>2</sub> and TiO<sub>2</sub> coatings had little effect on *R*<sub>0</sub>, but they increased the *R*<sub>EEL</sub>. Additionally, the ZrO<sub>2</sub> coating increased the *R*<sub>ct</sub>, while the TiO<sub>2</sub> coating decreased the resistance. The effect of different metal oxides coatings on the impedance of the LiCoO<sub>2</sub> electrode has been reported before [3–5]. The slightly increased *R*<sub>EEL</sub> was attributed to either

**Figure 4** Cyclic voltammetry of **a** pristine LiCoO<sub>2</sub>, **b** TiO<sub>2</sub>-coated LiCoO<sub>2</sub>, and **c** ZrO<sub>2</sub>-coated LiCoO<sub>2</sub> at different scan rates. **d** The evolution of peak current with respect to scan rate for different samples. Both TiO<sub>2</sub> and ZrO<sub>2</sub> coating slightly increase the diffusion coefficients of Li in LiCoO<sub>2</sub>.



poor  $\text{Li}^+$  transport through the EEI layer after the  $\text{TiO}_2/\text{ZrO}_2$  coating or the formation of a thicker EEI layer because of the coating. The decreased/increased  $R_{\text{ct}}$  of the  $\text{LiCoO}_2$  electrode after the  $\text{TiO}_2/\text{ZrO}_2$  coating could be attributed to different side products on the surface of the electrode, which was generated by reactions between the coatings and electrolytes. The side products could affect the desolvation process at the interface of EEI and electrolyte as well as affect the charge-transfer process at the interface of EEI and electrolyte, leading to different  $R_{\text{ct}}$ .

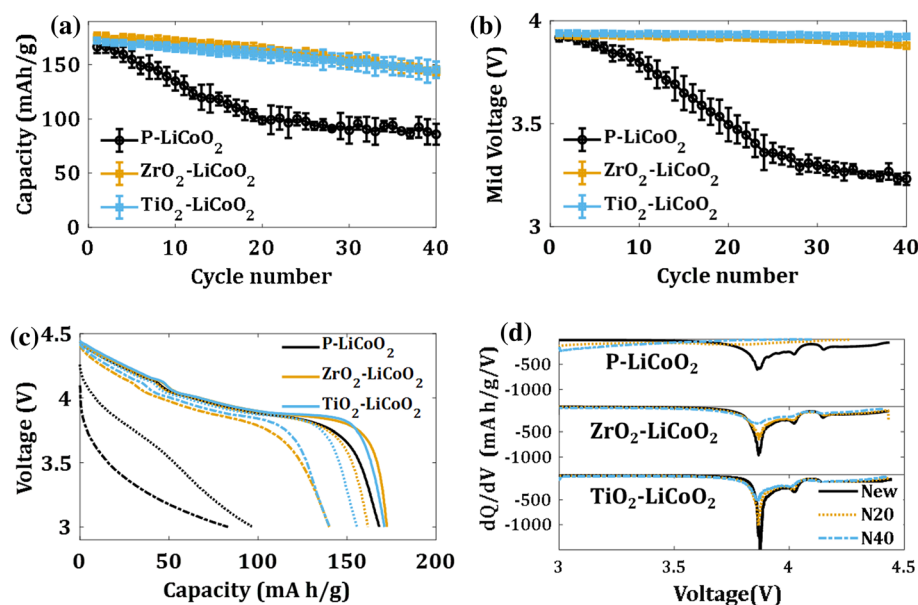
### Influence of MWR-synthesized $\text{TiO}_2/\text{ZrO}_2$ coatings on cycling stability of $\text{LiCoO}_2$ electrodes

The 4.5 V high-voltage cycling stability of the  $\text{LiCoO}_2$  electrode was largely improved by the  $\text{TiO}_2$  and  $\text{ZrO}_2$  coatings. Figure 5a compares the evolution of specific capacity for the three types of  $\text{LiCoO}_2$  electrodes during the cycling test. The result shows that the  $\text{TiO}_2$  and  $\text{ZrO}_2$  coatings significantly reduced the rate of capacity degradation. The  $\text{ZrO}_2$  coating improved the capacity remaining from 52.8 to 81.9% after 40 cycles, while the  $\text{TiO}_2$  coating improved it to 84.4%. Such improvement is battery than many of the existing studies, especially for the  $\text{TiO}_2$  coating (Table S3). The middle voltage of a cell is the voltage at the half of the discharge capacity, which represents the kinetic properties of the cell. Figure 5b shows that the

middle voltage of the pristine  $\text{LiCoO}_2$  electrode decreased from 3.964 to 3.232 V after 40 cycles, while the  $\text{ZrO}_2$ -coated  $\text{LiCoO}_2$  electrode decreased from 3.968 to 3.878 V, and  $\text{TiO}_2$ -coated  $\text{LiCoO}_2$  electrode decreased from 3.968 to 3.924 V. Thus, the  $\text{TiO}_2$  and  $\text{ZrO}_2$  coatings reduced the capacity degradation rate and protected the kinetics of the  $\text{LiCoO}_2$  electrode during the high-voltage cycling test.

The effect of the  $\text{TiO}_2$  and  $\text{ZrO}_2$  coatings on the cycling stability of the  $\text{LiCoO}_2$  electrode was further investigated by comparing and analyzing discharge curves, as shown in Fig. 5c, d. Figure 5c displays the discharge curves of the three types of  $\text{LiCoO}_2$  electrodes at different aging statuses. The discharge curves of the pristine  $\text{LiCoO}_2$  electrode showed a large drop in voltage and specific capacity after 20 (N20) and 40 cycles (N40). Moreover, the discharge plateaus almost disappeared in the discharge curves on N20 and N40. However, both the  $\text{TiO}_2$  and  $\text{ZrO}_2$  coatings reduced the decrease in the voltage and the specific capacity of the  $\text{LiCoO}_2$  electrode after 20 and 40 cycles. Additionally, the coatings maintained the discharge plateaus after the cycling test. Figure 5d compares the incremental capacity analysis (ICA) curves of the three  $\text{LiCoO}_2$  electrodes at different aging statuses. An ICA peak corresponds to a plateau in a discharge curve, which represents a phase transition process in the  $\text{LiCoO}_2$  electrode. Before the cycling test, three peaks could be identified for all  $\text{LiCoO}_2$  electrodes at around 4.15, 4.03, and 3.87 V. The intensity of a peak could be affected by the

**Figure 5** High-voltage (4.5 V) cycling stability of different  $\text{LiCoO}_2$  electrodes. **a** The capacity degradation of  $\text{LiCoO}_2$  electrodes. Three cells were tested for each type of electrode, and the distribution is shown in the error bar. **b** The evolution of the middle voltage for different  $\text{LiCoO}_2$  electrodes. **c** Discharge curves (C/2) of the  $\text{LiCoO}_2$  electrodes at new status, after 20 cycles, and after 40 cycles. **d** Incremental capacity analysis (ICA) for the discharge curves of  $\text{LiCoO}_2$  electrodes in plot (c).





cathode material and the homogeneous current distribution within the electrode. The higher ICA peak at 3.87 V in the TiO<sub>2</sub>-coated LiCoO<sub>2</sub> electrode suggests that the TiO<sub>2</sub> coating improved the homogeneity of current distribution in the LiCoO<sub>2</sub> electrode. This further agreed with the better rate performance of the TiO<sub>2</sub>-coated LiCoO<sub>2</sub> electrode seen in Fig. 3. After 20 and 40 cycles, all the ICA peaks of the pristine LiCoO<sub>2</sub> electrode disappeared, indicating either LiCoO<sub>2</sub> particles were destroyed that led to no phase transformations during the discharge process or largely inhomogeneous current distribution occurred in the electrode during discharge. In comparison, the ICA curves of both the ZrO<sub>2</sub>-coated and the TiO<sub>2</sub>-coated LiCoO<sub>2</sub> electrodes still showed three ICA peaks after 20 and 40 cycles. However, the locations of these peaks shifted to lower voltages and the intensities decreased after the cycling test, indicating the increase in cell resistance and the inhomogeneity of current distribution in these electrodes.

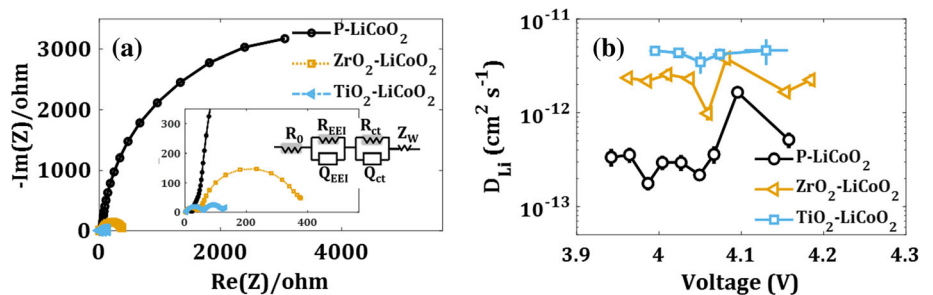
EIS measurements show that the TiO<sub>2</sub> and ZrO<sub>2</sub> coatings reduced the increase in the overall impedance of the LiCoO<sub>2</sub> electrode during the cycling test. Figure 6a compares the impedances of the three types of LiCoO<sub>2</sub> electrodes after 40 cycles. The charge-transfer resistance ( $R_{ct}$ ) in the pristine LiCoO<sub>2</sub> electrode became much larger than that in the TiO<sub>2</sub> and ZrO<sub>2</sub>-coated LiCoO<sub>2</sub> electrodes. This phenomenon has been reported inhibit the increase in  $R_{ct}$  in LiCoO<sub>2</sub> electrodes during cycling tests [25]. A second-order ECM was applied to quantitatively analyze the impedance, and the fitted results are listed in Table S2. The  $R_{ct}$  of the pristine LiCoO<sub>2</sub> increased by almost two orders of magnitude (80 times) after the cycling test, while the  $R_{ct}$  of the ZrO<sub>2</sub>-coated and TiO<sub>2</sub>-coated LiCoO<sub>2</sub> only increased by around 2.5 and 1.5 times, respectively. This might be from the formation of a passivation film on the surface of LiCoO<sub>2</sub>, like LiF, Li<sub>x</sub>PF<sub>y</sub>, and Li<sub>x</sub>PF<sub>y</sub>O<sub>z</sub>-type of compounds, which limited the charge-transfer

process of Li<sup>+</sup> at the cathode-electrolyte interface [26, 27]. The slow increase in  $R_{ct}$  in the TiO<sub>2</sub>/ZrO<sub>2</sub>-coated LiCoO<sub>2</sub> electrode suggested that the TiO<sub>2</sub> and ZrO<sub>2</sub> coatings could inhibit the formation of these compounds. Table S2 also suggests that the  $R_0$  did not increase after the cycling test for all the three LiCoO<sub>2</sub> electrodes, indicating that the electron transport pathways were maintained in these electrodes during the cycling test. Additionally, the  $R_{EEI}$  slightly decreased for all the three types of LiCoO<sub>2</sub> electrodes. The decreased  $R_{EEI}$  could be caused by the formation of cracks on the LiCoO<sub>2</sub> electrodes during the cycling test that increased the total surface area of the electrodes [26].

GITT data showed that the TiO<sub>2</sub> and ZrO<sub>2</sub> coatings helped maintain the kinetics of lithium transport in the LiCoO<sub>2</sub> particles during the cycling test. Figure 6b shows that the TiO<sub>2</sub>-coated LiCoO<sub>2</sub> electrode had the highest lithium diffusion coefficient ( $\sim 4.2 \cdot 10^{-12} \text{ cm}^2 \text{ S}^{-1}$ ) after cycling, which changed little from its initial status ( $\sim 5.5 \cdot 10^{-12} \text{ cm}^2 \text{ S}^{-1}$ ). Similarly, the lithium diffusion coefficient in the ZrO<sub>2</sub>-coated LiCoO<sub>2</sub> electrode decreased little after cycling (from  $\sim 4.0 \cdot 10^{-12} \text{ cm}^2 \text{ S}^{-1}$  to  $\sim 2.3 \cdot 10^{-12} \text{ cm}^2 \text{ S}^{-1}$ ). In comparison, the lithium diffusion coefficient in the pristine LiCoO<sub>2</sub> decreased by more than an order of magnitude after the cycling test (from  $\sim 4.0 \cdot 10^{-12}$  to  $\sim 2.3 \cdot 10^{-13} \text{ cm}^2 \text{ S}^{-1}$ ). This result suggests that the pristine LiCoO<sub>2</sub> particles went through severe damage during the cycling test, such as surface reconstruction caused by Co dissolution and channel blocking caused by the change of crystal structure on the surface [28]. These damages were reduced, if not eliminated, by the TiO<sub>2</sub> and ZrO<sub>2</sub> coatings according to the well-maintained lithium diffusion coefficients seen in the TiO<sub>2</sub>/ZrO<sub>2</sub>-coated LiCoO<sub>2</sub> electrodes.

The TiO<sub>2</sub> and ZrO<sub>2</sub> coating also reduced the Co dissolution from the LiCoO<sub>2</sub> electrode into the electrolyte, which is considered as one of the mechanisms

**Figure 6** Kinetics of LiCoO<sub>2</sub> electrode after the cycling test. **a** EIS results for the three types of LiCoO<sub>2</sub> electrodes. **b** The diffusion coefficient of Li in LiCoO<sub>2</sub> electrodes.



for capacity degradation of LiCoO<sub>2</sub> during cycling [29]. By applying the treatment described in the methodology section, we measured the concentration of Co element in the final electrolyte solution using ICP-MS technique. After the cycling test, the ratio of the dissolved Co to the total mass of the LiCoO<sub>2</sub> electrode was 0.76%, 0.12%, and 0.06% for the pristine LiCoO<sub>2</sub> electrode, the TiO<sub>2</sub>-coated LiCoO<sub>2</sub> electrode, and the ZrO<sub>2</sub>-coated LiCoO<sub>2</sub> electrode, respectively. Thus, the TiO<sub>2</sub> and ZrO<sub>2</sub> coating inhibited the dissolution of Co, which further explained the improved capacity remaining of the LiCoO<sub>2</sub> electrode after these coatings.

## Discussion

It is reported that the degradation of LiCoO<sub>2</sub> during cycling (below 4.5 V) is attributed to surface degradation effects rather than bulk degradation [30, 31]. This suggests the degradation rate could be related to the surface area of LiCoO<sub>2</sub> particles, i.e., the radius of the particle. Figure 7 summarizes the capacity fade rate of LiCoO<sub>2</sub> cycled at 4.5 V in recent papers. The figure suggests that the capacity fade rate increases with the decrease in the primary particle size. In our study, the LiCoO<sub>2</sub> particle size is 2 μm and the degradation rate of pristine LiCoO<sub>2</sub> is 1.18%/cycle. Our experiment data follows the trend of LiCoO<sub>2</sub> capacity fade rates reported in recent studies.

Additionally, our study shows that the degradation rate of LiCoO<sub>2</sub> is largely reduced by TiO<sub>2</sub> and ZrO<sub>2</sub>

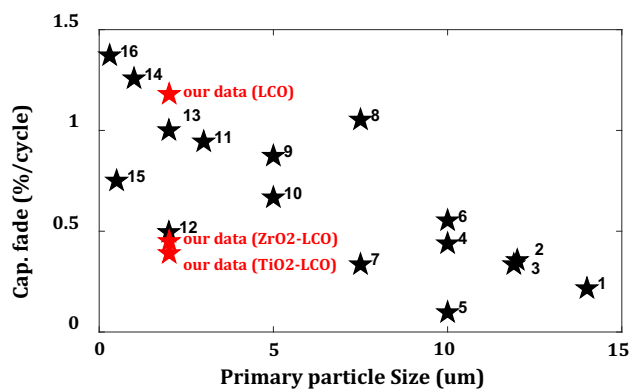


**Figure 7** Comparison 4.5 V high-voltage cycling performance of pristine LiCoO<sub>2</sub> with different particle sizes. Data are collected from recently published paper, as listed in Table S3. Our experiment data is highlighted by red, where LCO stands for pristine LiCoO<sub>2</sub> electrode and ZrO<sub>2</sub>/TiO<sub>2</sub>-LCO stands for ZrO<sub>2</sub>/TiO<sub>2</sub>-coated LiCoO<sub>2</sub> electrode.

coatings. Table 1 compares the effect of TiO<sub>2</sub> and ZrO<sub>2</sub> coatings on LiCoO<sub>2</sub> 4.5 V cycling performance via different techniques. Compared to existing literature, the ZrO<sub>2</sub>-coated LiCoO<sub>2</sub> in our study shows comparable cycling performance, while the TiO<sub>2</sub>-coated LiCoO<sub>2</sub> shows much better cycling stability.

XPS is a surface-sensitive spectroscopic technique that reveals not only the composition of the sample surface, but also the oxidation states of different elements present on the sample surface. Accordingly, we applied XPS to investigate the effect of the TiO<sub>2</sub> and ZrO<sub>2</sub> coatings on the electrochemical performance of the LiCoO<sub>2</sub> electrode. The TiO<sub>2</sub> coating affected the oxidation status of Co on the surface of LiCoO<sub>2</sub>, while the ZrO<sub>2</sub> coating had little effect. Figure 8a compares the binding energy of Co 2p peaks in LiCoO<sub>2</sub> powder before and after the TiO<sub>2</sub>/ZrO<sub>2</sub> coating via the MWR-assisted synthesis, followed by the heat treatment. The TiO<sub>2</sub>-coated LiCoO<sub>2</sub> powder before the heat treatment is also shown for comparison. Two XPS peaks at 780.0 eV and 780.46 eV were assigned to Co 2p<sub>3/2</sub>. The lower binding energy was from Co<sup>3+</sup> in LiCoO<sub>2</sub>, while the higher binding energy was from Co<sup>2+</sup> in Co(OH)<sub>2</sub> that formed on the surface of LiCoO<sub>2</sub> during air exposure [27]. The results show that the ZrO<sub>2</sub> coating did not affect the binding energies of Co 2p<sub>3/2</sub>, while the TiO<sub>2</sub> coating increased the Co<sup>3+</sup> peak from 780.0 to 780.18 eV and increased the Co<sup>2+</sup> peak from 780.46 to 780.63 eV. The increased binding energies for Co 2p<sub>3/2</sub> were not found in the TiO<sub>2</sub>-coated LiCoO<sub>2</sub> powder before the heat treatment, suggesting the heat treatment rather than the microwave processing affected the surface state of LiCoO<sub>2</sub> in the TiO<sub>2</sub>-coated LiCoO<sub>2</sub> powder. The little effect of the microwave processing on LiCoO<sub>2</sub> powder was also supported by analyzing the in situ XRD data in Fig. S9. The data suggests that the lattice parameter of LiCoO<sub>2</sub> did not change during the MWR-assisted synthesis of TiO<sub>2</sub> on the surface of LiCoO<sub>2</sub>.

Figure 8b compares the binding energy of Ti 2p in the TiO<sub>2</sub>-coated LiCoO<sub>2</sub> powder before and after the heat treatment. The results display that the Ti 2p<sub>2/3</sub> peak decreased from 458.40 to 458.06 eV after the heat treatment, suggesting that the heat treatment promoted interactions between Ti and Co on the surface of LiCoO<sub>2</sub>. One possible mechanism is that Ti diffused into the surface of LiCoO<sub>2</sub> lattice by either forming Ti interstitial or substituting Co [36]. This process affected the oxidation state of Co and Ti

**Table 1** Comparison of LiCoO<sub>2</sub> cycling stability at 4.5 V with TiO<sub>2</sub> and ZrO<sub>2</sub> coatings

Study	Coating	Technique	Cutoff voltage	Capacity fade rate improvement
Ref. [32]	TiO <sub>2</sub>	ALD	4.5 V	0.60 → 0.57%/cycle
Ref. [6]	TiO <sub>2</sub>	Sputtering	4.5 V	0.55 → 0.25%/cycle
Ref. [33]	TiO <sub>2</sub>	Sol-gel synthesis	4.5 V	2.4 → 1.40%/cycle
This study	TiO <sub>2</sub>	MWR	4.5 V	1.18 → 0.39%/cycle
Ref. [34]	ZrO <sub>2</sub>	Furnace heating	4.5 V	2.63 → 0.50%/cycle
Ref. [35]	ZrO <sub>2</sub>	Heat treatment	4.5 V	0.63 → 0.16%/cycle
This study	ZrO <sub>2</sub>	MWR	4.5 V	1.18 → 0.45%/cycle

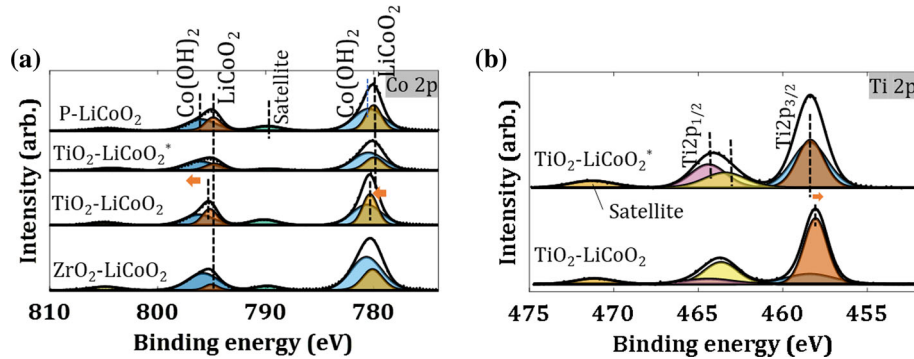


**Figure 8** X-ray photoelectron spectroscopy (XPS) measurement for different samples. **a** XPS spectroscopy of Co 2p in pristine LiCoO<sub>2</sub>, TiO<sub>2</sub>-coated LiCoO<sub>2</sub>, and ZrO<sub>2</sub>-coated LiCoO<sub>2</sub>. **b** The XPS spectroscopy of Ti 2p in TiO<sub>2</sub>-coated LiCoO<sub>2</sub> electrodes. The TiO<sub>2</sub>-LiCoO<sub>2</sub><sup>\*</sup> represents the TiO<sub>2</sub>-coated LiCoO<sub>2</sub> without heat

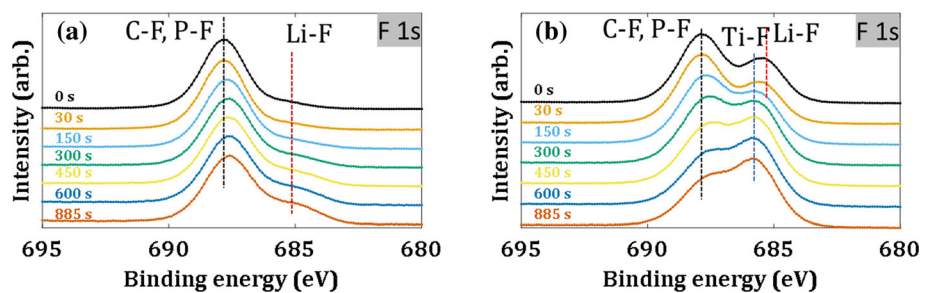
treatment. Measurement data (dots) are fitted by several individual spectra (colored regions). The combined spectra from these color shaded regions are shown as an envelope that matches well with experimental data (dots).

atoms and thus changed the binding energies of Co 2p<sub>3/2</sub> in LiCoO<sub>2</sub> and Ti 2p<sub>3/2</sub> in TiO<sub>2</sub>. However, the atomic radius of Zr (230 pm) is much bigger than Ti atom (147 pm), making Zr atom harder to diffuse into LiCoO<sub>2</sub> lattice. We believe that such a mechanism could also explain the different effects of the TiO<sub>2</sub> and ZrO<sub>2</sub> coatings on the diffusion coefficient of lithium in LiCoO<sub>2</sub> (Fig. 3c) as well as the rate capability of LiCoO<sub>2</sub> electrodes (Fig. 3a, b).

To understand the improved high-voltage cycling stability in the TiO<sub>2</sub>-coated LiCoO<sub>2</sub> electrode, XPS depth profiling was conducted for LiCoO<sub>2</sub> electrodes with and without the TiO<sub>2</sub> coating, after 40 cycles.

The results are shown in Fig. 9. The F 1s curve at 0s (no etching) could be roughly allocated into two peaks. The one at higher binding energy (~ 688 eV) was from fluoroorganic species, like C-F in PVDF, P-F in PF<sub>6</sub><sup>-</sup>, as well as other organic side products that contain fluoride, while the one at lower binding energy (~ 685 eV) was attributed to Li-F [27]. Compared with the fluoroorganic species peak, the Li-F peak in the pristine LiCoO<sub>2</sub> electrode was very weak and only showed up after 450 s of etching. Since many reports show that the passive film formed on battery electrodes is composed of an inner inorganic layer and an outer organic layer, the weak Li-F peak

**Figure 9** XPS measurement of F 1s binding energies for **a** pristine LiCoO<sub>2</sub> electrode, and **b** TiO<sub>2</sub>-coated LiCoO<sub>2</sub> electrode after 40 cycles. Dotted lines are used to label the possible fluoride compounds.



at 0 s indicated the formation of a relatively thick organic passivation film on the surface of the pristine LiCoO<sub>2</sub> after 40 cycles [37, 38].

In comparison, Fig. 9b shows strong Li–F peak before the etching treatment for the TiO<sub>2</sub>-coated LiCoO<sub>2</sub> electrode, suggesting a much thinner organic layer formed on the TiO<sub>2</sub>-coated LiCoO<sub>2</sub> electrode after the cycling test. Additionally, another peak at ~ 685.5 eV could be seen in the TiO<sub>2</sub>-coated LiCoO<sub>2</sub> electrode, especially after a few steps of the etching treatment. This peak has been assigned to metal fluoride in other studies and could be assigned to Ti–F here because TiO<sub>2</sub> is a Lewis base that reacts with trace HF in electrolyte [6]. After 150 s of the etching treatment, the Li–F peak disappeared and left only the Ti–F peak, implying that Ti–F dominated the fluoride components on the surface of TiO<sub>2</sub>-coated LiCoO<sub>2</sub> electrode. The formation of Ti–F consumed HF, which can be harmful to the cycling performance of battery electrolyte by leading to side reactions. Additionally, this metal fluoride layer is believed to have a higher chemical stability than the side products formed on the surface of the pristine LiCoO<sub>2</sub> [6]. This explained the phenomenon of less Co dissolution in the TiO<sub>2</sub>-coated LiCoO<sub>2</sub> electrode after the cycling test, which led to much better high-voltage cycling stability of the LiCoO<sub>2</sub> electrode after the TiO<sub>2</sub> coating.

## Conclusions

This study explores the microwave radiation (MWR)-assisted synthesis as a surface engineering technique to grow TiO<sub>2</sub> and ZrO<sub>2</sub> coatings on the surface of LIB electrodes like LiCoO<sub>2</sub>. This technique requires relatively short synthesis times and low synthesis temperature compared to traditional sol–gel and hydro/solvothermal synthesis methods. By selecting appropriate coating materials, like TiO<sub>2</sub>, we altered the surface characteristics of LiCoO<sub>2</sub> and improved its electrochemical performance. The capacity remaining was improved from 52.8 to 81.9% and 84.4% after 40 cycles by the ZrO<sub>2</sub> and TiO<sub>2</sub> coating, respectively. These results suggest that further attention should be given to synthesis under electromagnetic fields, because they provide promising, alternative routes to engineer the surface of battery electrodes for improving their performance. Exploring the synthesis of other materials via this process,

including both inorganic ceramics and organic polymers, will provide a novel pathway toward engineering advanced LIBs with high energy and power density, as well as extended lifespan.

## Acknowledgements

This work was supported by National Science Foundation (NSF) CAREER Award (CMMI1751605) and INCUBATE seed funding from Carnegie Mellon University. Microwave field-assisted TiO<sub>2</sub> synthesis efforts were supported by the DARPA AIRA Program (Grant Number HR00111990030). The authors acknowledge use of the Materials Characterization Facility at Carnegie Mellon University supported by Grant MCF-677,785. The Authors thank Dr. Joel Gillespie from the University of Pittsburgh Materials Characterization Laboratory for the access to the XPS spectrometer. Dr. Haiyan Wang and Ms. Xin Li Phuah acknowledge the support from the Office of Naval Research under Contract Nos. 1. N00014-17-1-2087 and N00014-16-1-2778. This research used 6-ID-D beamline and other resources in Advanced Photon Source, Argonne National Laboratory under Contract No. DE-AC02-06CH11357.

## Author contributions

LS contributed to conceptualization, experimental design, carrying out measurements, manuscript composition. SKJ helped in carrying out measurements. XLP involved in carrying out measurements. JX contributed to carrying out measurements. NN helped in experimental design, manuscript composition. HW helped in resources, funding acquisition. JSO contributed to resources. BRJ helped in supervision, experimental design, resources, manuscript composition, funding acquisition.

## Compliance with ethical standards

**Conflict of interest** All authors declare that they have no conflict of interest.

**Electronic supplementary material:** The online version of this article (<https://doi.org/10.1007/s10853-020-04871-5>) contains supplementary material, which is available to authorized users.

## References

- [1] Kalluri S, Yoon M, Jo M et al (2017) Surface engineering strategies of layered LiCoO<sub>2</sub> cathode material to realize high-energy and high-voltage Li-ion cells. *Adv energy mater* 7:1601507
- [2] Su L, Smith PM, Anand P et al (2018) Surface engineering of a LiMn<sub>2</sub>O<sub>4</sub> electrode using nanoscale polymer thin films via chemical vapor deposition polymerization. *ACS Appl Mater Inter* 10:27063–27073
- [3] Zhou A, Liu Q, Wang Y et al (2017) Al<sub>2</sub>O<sub>3</sub> surface coating on LiCoO<sub>2</sub> through a facile and scalable wet-chemical method towards high-energy cathode materials withstanding high cutoff voltages. *J Mater Chem A* 5:24361–24370
- [4] Dai X, Wang L, Xu J et al (2014) Improved electrochemical performance of LiCoO<sub>2</sub> electrodes with ZnO coating by radio frequency magnetron sputtering. *ACS Appl Mater Inter* 6:15853–15859
- [5] Dai X, Zhou A, Xu J et al (2015) Superior electrochemical performance of LiCoO<sub>2</sub> electrodes enabled by conductive Al<sub>2</sub>O<sub>3</sub>-doped ZnO coating via magnetron sputtering. *J Power Sour* 298:114–122
- [6] Zhou A, Lu Y, Wang Q et al (2017) Sputtering TiO<sub>2</sub> on LiCoO<sub>2</sub> composite electrodes as a simple and effective coating to enhance high-voltage cathode performance. *J Power Sour* 346:24–30
- [7] Zhou A, Xu J, Dai X et al (2016) Improved high-voltage and high-temperature electrochemical performances of LiCoO<sub>2</sub> cathode by electrode sputter-coating with Li<sub>3</sub>PO<sub>4</sub>. *J Power Sour* 322:10–16
- [8] Wang L, Chen B, Ma J et al (2018) Reviving lithium cobalt oxide-based lithium secondary batteries-toward a higher energy density. *Chem Soc Rev* 47:6505–6602
- [9] Jha, S. K.; Phuah, X. L.; Luo, J. et al. (2018), The effects of external fields in ceramic sintering., *J AM CERAM SOC*
- [10] Lidström P, Tierney J, Watheyb B et al (2001) Microwave assisted organic synthesis - a review. *Tetrahedron* 57:9225–9283
- [11] Nakamura, N.; Terban, M. W.; Billinge, S. et al. (2017), Unlocking the structure of mixed amorphous-crystalline ceramic oxide films synthesized under low temperature electromagnetic excitation., *J Mater Chem A*
- [12] Reeja-Jayan, B.; Harrison, K. L.; Yang, K. et al. (2012), Microwave-assisted Low-temperature Growth of Thin Films in Solution., *Sci Rep-UK* 2:
- [13] Bondioli F, Ferrari AM, Leonelli C et al (2001) Microwave-hydrothermal synthesis of nanocrystalline zirconia powders. *J Am Ceram Soc* 84:2728–2730
- [14] Shah JJ, Mohanraj K (2014) Comparison of conventional and microwave-assisted synthesis of benzotriazole derivatives. *Indian J Pharm Sci* 76:46
- [15] Kim KC, Jegal J, Bak S et al (2014) Improved high-voltage performance of FePO<sub>4</sub>-coated LiCoO<sub>2</sub> by microwave-assisted hydrothermal method. *Electrochem Commun* 43:113–116
- [16] Hoogenboom R, Schubert US (2007) Microwave-assisted polymer synthesis: recent developments in a rapidly expanding field of research. *Macromol Rapid Commun* 28:368–386
- [17] Su L, Tong P, Zhang L et al (2019) Photoelectrochemical immunoassay of aflatoxin B1 in foodstuff based on amorphous TiO<sub>2</sub> and CsPbBr<sub>3</sub> perovskite nanocrystals. *Analyst* 144:4880–4886
- [18] Shu J, Qiu Z, Lv S et al (2018) Plasmonic enhancement coupling with defect-engineered TiO<sub>2</sub>-x: a mode for sensitive photoelectrochemical biosensing. *Anal Chem* 90:2425–2429
- [19] Kim YJ, Cho J, Kim T et al (2003) Suppression of cobalt dissolution from the LiCoO<sub>2</sub> cathodes with various metal-oxide coatings. *J Electrochem Soc* 150:1723
- [20] Nakamura N, Seepaul J, Kadane JB et al (2017) Design for low-temperature microwave-assisted crystallization of ceramic thin films. *Appl Stoch Model Bus* 33:314–321
- [21] Jha SK, Charalambous H, Okasinski JS et al (2019) Using in operando diffraction to relate lattice strain with degradation mechanism in a NMC battery. *J Mater Sci* 54:2358–2370. <https://doi.org/10.1007/s10853-018-3007-8>
- [22] Jha SK, Nakamura N, Zhang S et al. (2019) Defect-mediated anisotropic lattice expansion in ceramics as evidence for nonthermal coupling between electromagnetic fields and matter. *Adv Eng Mater* 1900762
- [23] Nakamura NJ, Culbertson E, Billinge SJ et al. (2019) The role of defects in microwave-assisted synthesis of cubic ZrO<sub>2</sub>
- [24] Nam KM, Shim JH, Han D et al (2010) Syntheses and characterization of wurtzite CoO, rocksalt CoO, and spinel Co<sub>3</sub>O<sub>4</sub> nanocrystals: their interconversion and tuning of phase and morphology. *Chem Mater* 22:4446–4454
- [25] Sun Y, Han J, Myung S et al (2006) Significant improvement of high voltage cycling behavior AlF<sub>3</sub>-coated LiCoO<sub>2</sub> cathode. *Electrochem Commun* 8:821–826
- [26] Schulz N, Hausbrand R, Wittich C et al (2018) XPS-surface analysis of sei layers on Li-ion cathodes: part II. SEI-composition and formation inside composite electrodes. *J Electrochem Soc* 165:A833–A846
- [27] Schulz N, Hausbrand R, Dimesso L et al (2018) XPS-surface analysis of sei layers on Li-ion cathodes: Part I.

- Investigation of initial surface chemistry. *J Electrochem Soc* 165:A819–A832
- [28] Yang Z, Li R, Deng Z (2018) A deep study of the protection of lithium cobalt oxide with polymer surface modification at 4.5 V high voltage. *Sci Rep-UK*
- [29] Bai Y, Liu N, Liu J et al (2006) Coating Material-Induced Acidic Electrolyte Improves LiCoO<sub>2</sub> Performances. *Electrochem Solid-State Lett* 9:A552
- [30] Aurbach D, Markovsky B, Rodkin A et al (2002) On the capacity fading of LiCoO<sub>2</sub> intercalation electrodes: the effect of cycling, storage, temperature, and surface film forming additives. *Electrochim Acta* 47:4291–4306
- [31] Miyashiro H, Yamanaka A, Tabuchi M et al (2006) Improvement of degradation at elevated temperature and at high state-of-charge storage by ZrO<sub>2</sub> coating on LiCoO<sub>2</sub>. *J Electrochem Soc* 153:A348–A353
- [32] Cheng H, Wang F, Chu JP et al (2012) Enhanced cycleability in lithium ion batteries: resulting from atomic layer deposition of Al<sub>2</sub>O<sub>3</sub> or TiO<sub>2</sub> on LiCoO<sub>2</sub> electrodes. *J Phys Chem C* 116:7629–7637
- [33] Jayasree SS, Nair S, Santhanagopalan D (2018) Ultrathin TiO<sub>2</sub> coating on LiCoO<sub>2</sub> for improved electrochemical performance as Li-ion battery cathode. *CHEMISTRYSELECT* 3:2763–2766
- [34] Hwang BJ, Chen CY, Cheng MY et al (2010) Mechanism study of enhanced electrochemical performance of ZrO<sub>2</sub>-coated LiCoO<sub>2</sub> in high voltage region. *J Power Sour* 195:4255–4265
- [35] Chung KY, Yoon W, Lee HS et al (2006) In situ XRD studies of the structural changes of ZrO<sub>2</sub>-coated LiCoO<sub>2</sub> during cycling and their effects on capacity retention in lithium batteries. *J Power Sour* 163:185–190
- [36] Yu J, Han Z, Hu X et al (2014) The investigation of Ti-modified LiCoO<sub>2</sub> materials for lithium ion battery. *J Power Sou* 262:136–139
- [37] Zhang J, Wang R, Yang X et al (2012) Direct observation of inhomogeneous solid electrolyte interphase on MnO anode with atomic force microscopy and spectroscopy. *Nano Lett* 12:2153–2157
- [38] Kerlau M, Kostecki R (2006) Interfacial impedance study of Li-ion composite cathodes during aging at elevated temperatures. *J Electrochem Soc* 153:1644

**Publisher's Note** Springer Nature remains neutral with regard to jurisdictional claims in published maps and institutional affiliations.